Modeling heat transfer within porous multiconstituent materials

Mathieu Niezgoda, Denis Rochais, Franck Enguehard, Benoit Rousseau, Patrick Echegut

Journal of Physics: Conference Series **369** (2012) 012001 doi:10.1088/1742-6596/369/1/012001

Modeling heat transfer within porous multiconstituent materials

Mathieu NIEZGODA[1], Denis ROCHAIS[1], Franck ENGUEHARD[1], Benoit ROUSSEAU[2], Patrick ECHEGUT[3]

[1]Commissariat à l'Énergie Atomique et aux Énergies Alternatives, DAM, CEA Le Ripault, BP 16, 37260 MONTS, France
[2]Laboratoire de Thermocinétique de Nantes (LTN), CNRS UMR 6607, 44306 NANTES, France
[3]Conditions Extrêmes et Matériaux : Hautes Températures et Irradiation (CEMHTI), CNRS UPR 3079, 45071 ORLÉANS, France

denis.rochais@cea.fr

Abstract. The purpose of our work has been to determine the effective thermal properties of materials considered heterogeneous at the microscale but which are regarded as homogenous in the macroscale environment in which they are used. We have developed a calculation code that renders it possible to simulate thermal experiments over complex multiconstituent materials from their numerical microstructural morphology obtained by volume segmentation through tomography. This modeling relies on the transient solving of the coupled conductive and radiative heat transfer in these voxelized structures.

1. Nomenclature

c_p	massic specific heat $(J.kg^{-1}.K^{-1})$	*Greek symbols*	
$\mathscr{D}$	Dirac function (s^{-1})	δ	voxel thickness (m)
$\mathscr{C}$	conductance $(W.m^{-1})$	Δt	step of time (s)
$\mathscr{E}$	total intensity of the black body $(W.m^{-2})$	κ	absorption coefficient (m^{-1})
$\mathcal{E}$	set of voxels	λ_i	conductivity $(W.m^{-1}.K^{-1})$
E	energy (J)	λ	wavelength (m)
f	form ratio	ϕ	flux (W)
F	form ratio with absorption	φ	flux density $(W.m^{-2})$
$\mathbf{F}$	function (vector) of the equations	ρ	density $(kg.m^{-3})$
$\mathbf{F}'$	jacobian matrix of $\mathbf{F}$	ρ_{ij}	reflectivity
$\mathcal{F}_{\text{up}}$	voxels of the superior face	σ_{SB}	Stefan-Boltzmann constant
h	convecto-radiative coefficient $(W.m^{-2}.K^{-1})$	θ	angle
$I, \mathscr{I}$	intensity $(W.m^{-2})$ or $(W.m^{-2}.sr^{-1})$	τ_{ij}	transmitivity

I^0	total intensity of the black body $(W.m^{-2})$	*Subscripts and superscripts*	
k	extinction index	$'$	directional parameter
M	intensities arrival point	=	matrix
n	optical index	amb	ambiante
N	intensities origin point	i, j, k	voxel locations or face
s	curvilign abscisse (m)	cond	conductif
S	voxel face	e	incoming
$\mathcal{S}$	set of edges voxels	λ	spectral parameter
t	time (s)	n	iteration or step time
T	temperature (K)	O	opposite faces
$\mathbf{X}$	intensities and temperature vector	r, rad	radiative
z	axial coordinate	s	outcoming
		V	adjacent faces

2. Introduction

The French Atomic Energy Commission (CEA) works a great deal with porous materials – carbon composites, ceramics – and aims to optimize their microstructural and thermal properties for specific uses. A material of interest can be composed of several constituents and generally has a complex structure. Its pore size range can be quite large (several tens of micrometers). It is used in large-scale systems that are bigger than its own characteristic scale and can be submitted to very high fluxes and temperatures (until 3000°C). In these conditions, the material is considered as equivalent to a homogeneous medium for the simulation of its behavior in its using environment. Its local morphology is thus not taken into account.

We are therefore interested in characterizing the effective thermal properties of materials with heterogeneous microstructural morphologies. The objective is to determine the properties that theses materials would have if they were homogeneous. In order to do so, we have developed a methodology that consists in starting from a 3D-microstructure of the studied materials obtained by X-microtomography or FIB/SEM-tomography. The observations of the representative rebuilt volumes enable an understanding and analysis of the structural organization of these materials. The microstructures constitute the numerical support to compute the numerical experiment simulations.

The results render it possible to estimate the thermal properties of the materials in question. We are especially interested in the effective thermal diffusivity of porous multiconstituent materials that we estimate as a function of temperature with the help of an inverse method applied to experimental thermograms obtained by the flash method [1]. However, the identification of the diffusivity of porous and/or semitransparent materials is made difficult because of the thermal behavior of these media in which a strong conducto-radiative coupling can quickly occur when the temperature increases. For this reason, we have modeled the coupled conductive and radiative heat transfer as a function of the temperature within porous multiconstituent materials from their morphology discretized into a set of homogeneous voxels. The size of the voxel is larger than the wavelength which is the case in practice because of the studied materials and the high temperature. This modeling rendered it possible, on the one hand, to simulate any kind of numerical thermal experiments, especially the flash method, and on the other hand, to reproduce the thermal behavior of our materials in their using conditions. Our modeling is only accurate in the context we have here presented.

Considering the coupled heat transfer in porous media is very difficult to take into account, already in a homogeneous medium and even more in an inhomogeneous one, because it strongly depends on the microstructure of the constituents. Consequently, the media are mainly studied at ambient temperature where the conductive transfer is dominating and the radiation neglected or they are interested in their radiative properties and only the radiation is considered. Some researchers estimated

the effective thermal conductivity especially in foams [2–3] often by being based on analytical model of the porous structure. Other works deal with only the radiative heat transfer [4–5]. Thus, very few studies deal with the coupled heat transfer in porous media at high temperatures. But the flash method was modeled in the case of a coupled conductive and radiative heat transfer within a semi-transparent material [1, 6–9].

Moreover, among the works dealing with the conductive or radiative heat transfer, most of them concerns 1D-problems and a weaker number focus on the numerical microstructure of the sample obtained by 3D-X-ray tomography. Numerical methods were developed to estimate the effective thermal conductivity [10–12] and they were applied to 3D-microstructures obtained by X-ray-tomography [13]. At the same time, the radiative properties (extinction and absorption coefficients, scattering phase function, etc.) were investigated starting from the microstructure [14–15] and thanks to the X-ray tomography [16–21].

Finally, in our knowledge, there is no study looking into the modeling of the coupled conductive and radiative heat transfer from the 3D-microstructure of porous media as a function of the temperature.

The purpose of this paper consists in describing the modeling approach and explaining the analytical and numerical resolution of this thermal problem. We have demonstrated how to solve the flash method in such voxelized structures and how to organize the analytical resolution of this problem to compute it in a calculation code giving the transient temperature field in each voxel. Furthermore, we have enumerated all the thermophysical and radiative data introduced in the developed calculation code for each constituent at the voxel scale to carry out our simulations. Finally, we have obtained the first validation results of the code.

3. Solving the flash method in a voxelized structure

3.1. Obtaining the microstructural morphology of materials

First, a numerical volume of the studied sample is required as the support of the numerical thermal experiment simulation [22]. By using the X-microtomography or FIB/SEM-tomography technique over the sample, it is possible to obtain a set of 2D images from which the sample can be built in 3D and then discretized into a set of voxels. These voxels constitute the elementary mesh over which the considered heat transfer problem is solved. Each voxel is therefore assumed to be homogeneous with the properties of the constituent of which it is composed. This discretization is a very fine description of the morphology of the studied samples. We have to make sure that the size of the voxels is larger than the wavelength of the occurring radiation. It is the case in the context of our study and we present what follows in the next parts.

3.2. Analytical solving

Consider a multiconstituent sample, representative of the studied material, in the form of a parallelepiped some millimeters long. It is composed of cubic homogeneous voxels. Each voxel – with a size of a few tens of microns– is attributed the thermophysical and radiative properties of the material that it represents and can be semi-transparent. The upper face of the sample is submitted to a pulsed energy deposition of short duration at $t = 0$, which is assumed to be uniform over the surface. This face and the opposite one are submitted to heat dissipation through a coupled convecto-radiative coefficient. Moreover, these two faces are assumed to be opaque with emission and diffuse reflection. The lateral walls are assumed to be adiabatic and totally reflective.

The physics of this thermal problem are governed by two highly coupled equations: the radiative transfer equation and a flux balance equation. We need to solve these two equations in each voxel to model the heat transfer in the previously presented problem. To simplify a complex mathematical problem, the following assumptions are made. (*i*) For each face of each voxel, the intensities are assumed to be isotropic in each half-space. Two intensities are therefore considered (back and front) for each face. (*ii*) The radiative properties and variables of each constituent are presumed to be

independent of the wavelength (grey media). This is done in order to consider mean radiative properties and variables. Such an assumption, although it may seem strong, is nevertheless legitimate because the sought temperature field is the result of energetic variables issued from the integration of all the contributions of each wavelength. And (*iii*) the properties are assumed to be independent of the temperature since the increase in temperature range is small in the case of the flash method. When it comes to real materials, they can be subjected to greater thermal stresses. This is accounted for by making their properties vary as a function of the temperature.

Thus, we have thirteen unknowns in each voxel (and we especially seek to determine the time-resolved temperature field of each voxel): the temperature and twelve intensities. For each voxel, we solve the radiative transfer equation between each face and the five others (i.e., six equations), as well as the flux balance equation involving the conductive and radiative flux exchanged by the voxel with its six neighbors (i.e., one equation). The mathematical problem is closed with six interface equations – one on each face – relating the incoming intensity on the face of the voxel to the outgoing one of its neighbor at the same face. In order to determine these thirteen unknowns, we need to simultaneously solve these thirteen equations.

3.3. The radiative transfer equation

Consider a voxel as it was previously described. Its faces are arbitrarily numbered as presented in Figure 1. We want an expression of the intensity going outside through one of the faces (for example the face numbered 6) which is obtained by adding the contributions of the intensities going inside through the five other faces. It is likely that the intensity going outside through face 6 is not isotropic.

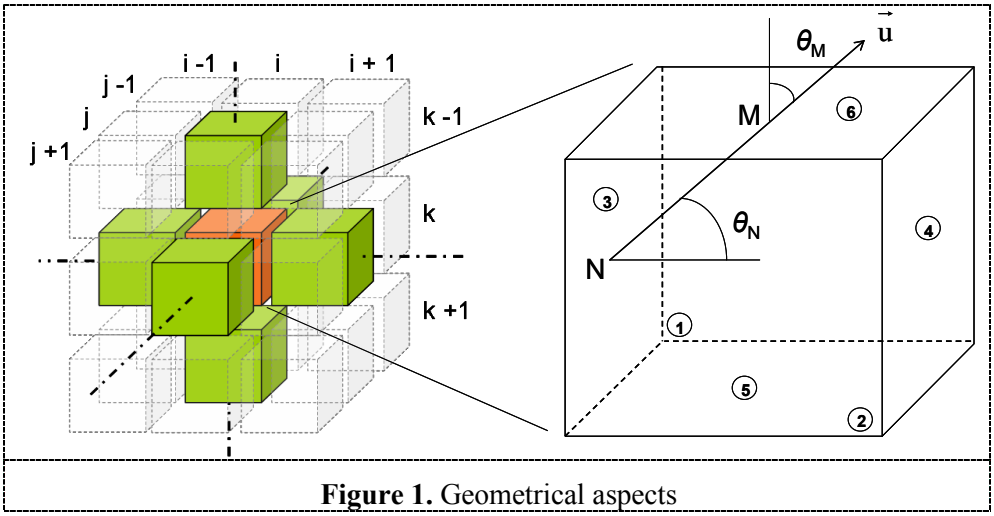

Figure 1. Geometrical aspects

Thus, the radiative flux going outside through this face is sought and the equivalent isotropic intensity going inside is deduced.

$$\phi_6^s = \iint_{M\in S_6} \overrightarrow{\varphi_r^s}(M)\cdot\vec{z}\,\mathrm{d}S_{M_6} \quad \text{where:} \quad \overrightarrow{\varphi_r^s} = \sum_{i=1}^{5} \iint_{N_i\in S_i} I'\left(M;\frac{\overrightarrow{N_iM}}{N_iM}\right)\frac{\overrightarrow{N_iM}}{N_iM}\frac{\cos\theta_{N_i}}{N_iM^2}\,\mathrm{d}S_{N_i} \tag{1}$$

To determine the directional intensity in M in the direction of **u**, the RTE is applied to the voxel between N and M. As the voxel is homogeneous, there is no scattering within each voxel. Thus, we only study materials in which there would not be micro- or nano-porosity and consequently scattering within the voxels. But scattering appears at the sample scale because of its heterogeneity. Indeed, if a voxel has a neighbour of different nature, a part of the outgoing radiative transfer is reflected whereas an other part is transmitted. At a larger scale (the one of the sample), that causes scattering. Under the assumption of grey medium, it is written:

$$\frac{\mathrm{d}I'(s_i)}{\mathrm{d}s_i} + \kappa I'(s_i) = \kappa I^0(T) \quad \text{with:} \quad I^0(T) = \frac{n^2 \sigma_{\mathrm{SB}} T^4}{\pi} = \mathscr{E} \tag{2}$$

It is simply solved, giving:

$$I'(s_i) = (\mathscr{I}_i^{\mathrm{e}} - \mathscr{E})\, \mathrm{e}^{-\kappa \cdot N_i M} + \mathscr{E} \tag{3}$$

where $\mathscr{I}_i^{\mathrm{e}}$ is the (isotropic) intensity going inside through face *i*. After some easy calculations, it is deduced that:

$$\phi_6^{\mathrm{s}} = \iint_{M \in S_6} \sum_{i=1}^{5} \left[(\mathscr{I}_i^{\mathrm{e}} - \mathscr{E}) \iint_{N_i \in S_i} \mathrm{e}^{-\kappa \cdot N_i M} \frac{\cos\theta_M \cos\theta_{N_i}}{N_i M^2} \,\mathrm{d}S_{N_i} + \mathscr{E} \iint_{N_i \in S_i} \frac{\cos\theta_M \cos\theta_{N_i}}{N_i M^2} \,\mathrm{d}S_{N_i} \right] \mathrm{d}S_M \tag{4}$$

Hence:

$$\phi_6^{\mathrm{s}} = \sum_{i=1}^{5} \left[(\mathscr{I}_i^{\mathrm{e}} - \mathscr{E}) \iint_{M \in S_6} \iint_{N_i \in S_i} \mathrm{e}^{-\kappa \cdot N_i M} \frac{\cos\theta_M \cos\theta_{N_i}}{N_i M^2} \,\mathrm{d}S_{N_i} \,\mathrm{d}S_M \right] + \mathscr{E} \pi \delta^2 \underbrace{\sum_{i=1}^{5} f_{6i}}_{=1} \tag{5}$$

where f_{ij} is the form ratio of which the sum on the five faces gives 1. Similarly to the form ratio, a dimensionless parameter is defined which is called the form ratio with absorption F_{ij}.

$$F_{ij} = \frac{1}{\pi S_i} \iint_{M_i \in S_i} \iint_{N_j \in S_j} \mathrm{e}^{-\kappa \cdot N_j M_i} \frac{\cos\theta_{M_i} \cos\theta_{N_j}}{N_j {M_i}^2} \,\mathrm{d}S_{N_j} \,\mathrm{d}S_{M_i} \tag{6}$$

By setting an equality between the equivalent isotropic intensity going outside through face 6 and equation 5, we finally obtain:

$$\phi_6^{\mathrm{s}} = \pi \delta^2 \mathscr{I}_6^{\mathrm{s}} = \pi \delta^2 \left[\sum_{i=1}^{5} (\mathscr{I}_i^{\mathrm{e}} - \mathscr{E})\, F_{6i} + \mathscr{E} \right] \tag{7}$$

$$\mathscr{I}_6^{\mathrm{s}} = \sum_{i=1}^{5} (\mathscr{I}_i^{\mathrm{e}} - \mathscr{E})\, F_{6i} + \mathscr{E} \tag{8}$$

We can show by geometrical considerations that the thirty-six form ratios with absorption can be reduced in two. We now have: $F_{61} = F_{62} = F_{63} = F_{64} = F_{\mathrm{V}}$ and $F_{65} = F_{\mathrm{O}}$. These form ratios with absorption depend only on the optical thickness $\kappa\delta$ in the case of a homogeneous cubic voxel and are constant and particular to a material.

Finally, here are the six first equations for a voxel:

$$\begin{aligned}
\mathscr{I}_1^{\mathrm{s}} &= F_{\mathrm{V}} \sum_{i=3}^{6} \mathscr{I}_i^{\mathrm{e}} + F_{\mathrm{O}} \mathscr{I}_2^{\mathrm{e}} + \mathscr{E}(1 - F_{\mathrm{O}} - 4F_{\mathrm{V}}) \\
\mathscr{I}_2^{\mathrm{s}} &= F_{\mathrm{V}} \sum_{i=3}^{6} \mathscr{I}_i^{\mathrm{e}} + F_{\mathrm{O}} \mathscr{I}_1^{\mathrm{e}} + \mathscr{E}(1 - F_{\mathrm{O}} - 4F_{\mathrm{V}}) \\
\mathscr{I}_3^{\mathrm{s}} &= F_{\mathrm{V}}(\mathscr{I}_1^{\mathrm{e}} + \mathscr{I}_2^{\mathrm{e}} + \mathscr{I}_5^{\mathrm{e}} + \mathscr{I}_6^{\mathrm{e}}) + F_{\mathrm{O}} \mathscr{I}_4^{\mathrm{e}} + \mathscr{E}(1 - F_{\mathrm{O}} - 4F_{\mathrm{V}}) \\
\mathscr{I}_4^{\mathrm{s}} &= F_{\mathrm{V}}(\mathscr{I}_1^{\mathrm{e}} + \mathscr{I}_2^{\mathrm{e}} + \mathscr{I}_5^{\mathrm{e}} + \mathscr{I}_6^{\mathrm{e}}) + F_{\mathrm{O}} \mathscr{I}_3^{\mathrm{e}} + \mathscr{E}(1 - F_{\mathrm{O}} - 4F_{\mathrm{V}}) \\
\mathscr{I}_5^{\mathrm{s}} &= F_{\mathrm{V}} \sum_{i=1}^{4} \mathscr{I}_i^{\mathrm{e}} + F_{\mathrm{O}} \mathscr{I}_6^{\mathrm{e}} + \mathscr{E}(1 - F_{\mathrm{O}} - 4F_{\mathrm{V}}) \\
\mathscr{I}_6^{\mathrm{s}} &= F_{\mathrm{V}} \sum_{i=1}^{4} \mathscr{I}_i^{\mathrm{e}} + F_{\mathrm{O}} \mathscr{I}_5^{\mathrm{e}} + \mathscr{E}(1 - F_{\mathrm{O}} - 4F_{\mathrm{V}})
\end{aligned} \tag{9-14}$$

The form ratios with absorption can be written in the following way:

$$F_{\mathrm{O}} = \int_{x=0}^{1}\int_{y=0}^{1}\int_{z=0}^{1}\int_{t=0}^{1} \frac{\mathrm{e}^{-\kappa\delta\sqrt{(x-z)^2+(y-t)^2+1}}}{\left((x-z)^2+(y-t)^2+1\right)^2}\,\mathrm{d}x\,\mathrm{d}y\,\mathrm{d}z\,\mathrm{d}t$$
$$F_{\mathrm{V}} = \int_{x=0}^{1}\int_{y=0}^{1}\int_{z=0}^{1}\int_{t=0}^{1} zt\frac{\mathrm{e}^{-\kappa\delta\sqrt{(y-x)^2+z^2+t^2}}}{\left((y-x)^2+z^2+t^2\right)^2}\,\mathrm{d}x\,\mathrm{d}y\,\mathrm{d}z\,\mathrm{d}t \qquad (15\text{-}16)$$

Multiple integral calculations render it possible to simplify these quadruple integrals into a simple one:

$$F_{\mathrm{O}} = \frac{2}{\pi}\int_{0}^{1}\frac{\mathrm{e}^{-\kappa\delta\sqrt{r^2+1}}}{(r^2+1)^2}r(\pi-4r+r^2)\,\mathrm{d}r + \frac{2}{\pi}\int_{1}^{\sqrt{2}}\frac{\mathrm{e}^{-\kappa\delta\sqrt{r^2+1}}}{(r^2+1)^2}r\left(\pi-2-r^2+4\sqrt{r^2-1}-4\arccos\left(\frac{1}{r}\right)\right)\mathrm{d}r$$

$$F_{\mathrm{V}} = \frac{8\kappa\delta-3+(3-5\kappa\delta)\mathrm{e}^{-\kappa\delta}}{12\pi(\kappa\delta)^2}+\frac{1}{12\pi}\int_{1}^{\sqrt{2}}\frac{\mathrm{e}^{-\kappa\delta r}}{r^3}\left(6r^4-6r^2+5-16(r^2-1)^{\frac{3}{2}}\right)\mathrm{d}r + \frac{1}{12\pi}\int_{\sqrt{2}}^{\sqrt{3}}\frac{\mathrm{e}^{-\kappa\delta r}}{r^3}\left(-3r^4+6r^2+1+8(r^2-2)^{\frac{3}{2}}\right)\mathrm{d}r \qquad (17\text{-}18)$$

We can also write an intensity continuity relation at each face of each voxel (six extra equation for each voxel). For example, the intensity going inside through face 6 is the sum of the transmitted part of the intensity going outside through face 5 of the upper voxel and of the reflected part of the intensity going outside through face 6 of the considered voxel.

$$\begin{aligned}
\mathscr{I}_1^{\mathrm{e}}(i,j,k) &= \rho_{12'}\mathscr{I}_1^{\mathrm{s}}(i,j,k) + \tau_{2'1}\mathscr{I}_2^{\mathrm{s}}(i-1,j,k)\\
\mathscr{I}_2^{\mathrm{e}}(i,j,k) &= \rho_{21'}\mathscr{I}_2^{\mathrm{s}}(i,j,k) + \tau_{1'2}\mathscr{I}_1^{\mathrm{s}}(i+1,j,k)\\
\mathscr{I}_3^{\mathrm{e}}(i,j,k) &= \rho_{34'}\mathscr{I}_3^{\mathrm{s}}(i,j,k) + \tau_{4'3}\mathscr{I}_4^{\mathrm{s}}(i,j-1,k)\\
\mathscr{I}_4^{\mathrm{e}}(i,j,k) &= \rho_{43'}\mathscr{I}_4^{\mathrm{s}}(i,j,k) + \tau_{3'4}\mathscr{I}_3^{\mathrm{s}}(i,j+1,k)\\
\mathscr{I}_5^{\mathrm{e}}(i,j,k) &= \rho_{56'}\mathscr{I}_5^{\mathrm{s}}(i,j,k) + \tau_{6'5}\mathscr{I}_6^{\mathrm{s}}(i,j,k-1)\\
\mathscr{I}_6^{\mathrm{e}}(i,j,k) &= \rho_{65'}\mathscr{I}_6^{\mathrm{s}}(i,j,k) + \tau_{5'6}\mathscr{I}_5^{\mathrm{s}}(i,j,k+1)
\end{aligned} \qquad (19\text{-}24)$$

By eliminating intensities going outside in equations (19-24), the equations (9-14) enable to reduce the initial problem with thirteen unknowns for each voxel to a problem with seven unknowns for each voxel.

3.4. The flux balance

The last equation to be formulated is a flux balance: the sum of the conductive and radiative flux entering a voxel *i* contributes to increase its temperature.

$$\forall i \in \mathcal{E}\backslash\mathcal{S}, \qquad \sum_{k=1}^{6} \phi^i_{\mathrm{cond},k} + \sum_{k=1}^{6} \phi^i_{\mathrm{rad},k} = \rho c_p \delta^3 \frac{\partial T_i}{\partial t}$$

$$\forall i \in \mathcal{E}\backslash\mathcal{S}, \quad \sum_{k=1}^{6} \underbrace{\frac{2\delta\lambda_i\lambda_k}{\lambda_i+\lambda_k}}_{\mathscr{C}_{i/k}} \left(T_k^{n+1} - T_i^{n+1}\right) + \pi\delta^2 \sum_{k=1}^{6} \left(\mathscr{I}_k^{\mathrm{e}^i} - \mathscr{I}_k^{\mathrm{s}^i}\right) - \rho c_p \delta^3 \frac{T_i^{n+1} - T_i^n}{\Delta t} = 0 \tag{25-26}$$

3.5. Boundary conditions

The equations mentioned above are valid for all the problems that can be studied with this modeling approach. Only the equations related to the boundary conditions, concerning the voxels belonging to the six faces of the parallelepiped volume, the twelve sides and the eight corners, can change from one problem to another. In the case of the flash method, in order to take into account the boundary conditions of the lateral walls, the previous equations have to be adjusted for the concerned voxels in the sense that there is no radiation transmitted outside the sample but rather that it is totally reflected on the lateral walls (i.e., the intensities entering and exiting are equal). Moreover, there is neither a conductive flux, nor a radiative one (with the previous consideration) going inside through these walls. In the case of the boundary conditions on the upper and lower walls, we have that at the lower/upper wall of each concerned voxel, the intensity going inside through these face is equal to the black body intensity at the same temperature. Moreover, a flux balance at the wall of each voxel can be written: thus, in the upper face, the sum of the conductive and radiative flux going inside is equal to the flux brought by the flash and exchanged by the convective and radiative dissipation:

$$\begin{aligned} \forall i \in \mathcal{F}_{\mathrm{up}} : \qquad & \phi_{\mathrm{cond}} + \phi_{\mathrm{rad}} = \phi_{\mathrm{flash}} - \phi_{\mathrm{losses}} \\ 2\lambda_i\delta\left(T_{\mathrm{wall}} - T_i\right) + \pi\delta^2 & \left(\mathscr{I}_6^{\mathrm{e}^i} - \mathscr{I}_6^{\mathrm{s}^i}\right) = E_{\mathrm{flash}}\delta^2\mathscr{D}(t) - h\delta^2\left(T_{\mathrm{wall}} - T_{\mathrm{amb}}\right) \end{aligned} \tag{27}$$

Because of these last considerations, the temperatures at the lower/upper faces of the voxels on the lower/upper walls also have to be considered as unknowns in the problem.

3.6. Computation and numerical solving

X is the vector holding all the unknowns of the problem *i.e.,* seven times the number of voxels. This vector is the solution of a non-linear equation that can be written **F(X)** = **0** and that is solved numerically by Newton's iteration method for systems of 2nd or superior dimension according to:

$$\overline{\overline{\mathbf{F}'}}(\mathbf{X}_n)\left[\mathbf{X}_n - \mathbf{X}_{n+1}\right] = \mathbf{F}(\mathbf{X}_n) \quad \text{where :} \quad \overline{\overline{\mathbf{F}'}}(\mathbf{X}) = \left(\frac{\partial F_i(\mathbf{X})}{\partial X_j}\right)_{i,j} \tag{28}$$

Since $\mathbf{X}_n$ is known, and with $\mathbf{Y}_n = \mathbf{X}_n - \mathbf{X}_{n+1}$, the numerical problem amounts to solving a linear system for each iteration of Newton's method until the convergence to the solution giving **X**. There is an incredible amount of data to stock in memory (especially the matrix $\mathbf{F}'(\mathbf{X}_n)$). To numerically solve these linear systems while avoiding keeping any data in memory, the iterative algorithm of Fletcher-Reeves (modified by Polak-Ribiere) has been chosen. It is easy to set up and very efficient in convergence speed.

Below is the procedure of the numerical solving of our problem. For each time step, Newton's iteration method was applied until the convergence of the sought vector **X** (whose components were initialized at the ones resulting from the previous time step or at arbitrarily assumed values for the first time step). For each iteration, the Polak-Ribiere algorithm was applied until the convergence of the vector **Y** (arbitrarily initialized) from which $\mathbf{X}_{n+1}$ was deduced since $\mathbf{X}_n$ was known. Finally, the components of **X** giving the temperature in each voxel for each time step rendered it possible to obtain the temperature field within the sample for the experiment, and especially a thermogram of the opposite face to the Dirac stimulation in the case of the flash method.

4. Thermophysical and radiative properties

The code presented in the previous part is a direct model making it possible to find an unknown parameter by calculation. Here, this was the transient temperature in each voxel. The different local thermophysical and radiative properties that are particular to each constituent of the sample have to be input in the code.

The voxel size is given by the tomography resolution. The volume specific heat is used for each constituent at the experiment temperature and these values were either found in the literature or measured by techniques of calorimetry existing in the laboratory. The thermal diffusivity from the micrometric scale to one of a few dozen micrometers was measured by photoreflectance and infrared microscopy as a function of the temperature [23].

The optical index and the absorption coefficient of the constituent were issued from spectral emission measures thanks to the infrared spectroscopy technique [24]. The emission spectrum of the constituent made it possible to determine, by means of the dielectric function, the spectrum of the real part and the imaginary part of the complex refraction index: the spectrum of the optical index and the extinction index, respectively (from which the absorption coefficient could be deducted). Considering the mean radiative properties over the entire spectrum, the optical indexes and the absorption coefficients were calculated from the obtained spectrum with the following definitions:

$$n = \frac{\int_0^{+\infty} n_\lambda I_\lambda^0(T)\,\mathrm{d}\lambda}{\int_0^{+\infty} I_\lambda^0(T)\,\mathrm{d}\lambda} \quad \text{and} \quad \kappa = \frac{\int_0^{+\infty} \kappa_\lambda I_\lambda^0(T)\,\mathrm{d}\lambda}{\int_0^{+\infty} I_\lambda^0(T)\,\mathrm{d}\lambda} \quad \text{with: } \kappa_\lambda = 4\pi\frac{k_\lambda}{\lambda} \tag{29}$$

Finally, the reflection (reflectivities) and transmission (transmitivities) coefficients were determined at the interface between the constituents by the Fresnel relation under collimated light. It was integrated over all the half-space since an isotropic diffuse radiation is considered.

5. Code validation

In order to validate the code for which we have presented the theoretical conception, we have attempted to compare the results it provides with data obtained with another calculation code. The considered experiment consisted of a stationary guarded hot plate technique. The code simulated the unidirectional coupled conductive and radiative heat transfer between two infinite plates for which the emissivity was known. One was at a low temperature (cold), the other at a higher one (hot). To solve the problem, the other code used a discrete ordinates method and an adaptive step of space.

To be close to this configuration, we considered a monocolumn structure composed of voxels from the same material. However, our configuration was not strictly 1D. For the sake of comparison, the lateral walls of our column had to be considered as at infinity, implying that the form ratios with absorption had to be recalculated with quite different expressions than the ones defined. They were thus function of the form ratios. We could show that the form ratios with absorption between adjacent faces were equal to zero when the lateral walls were at infinity, as were those between the opposite faces at infinity. The form ratio with absorption between the opposite faces in the direction of the heat transfer (perpendicular to the plates) was not equal to zero. Its value tends to 1 when the optical thickness $\kappa\delta$ tends to 0.

The case was the following. The hot wall temperature was 2000 K, and that of the cold wall was 1000 K. Their emissivity was 1, the thickness of the sample was 2 mm, and its conductivity was 2.5 $mW.m^{-1}.K^{-1}$. Figure 2 presents three temperature profiles for three values of the mean absorption coefficient (100, 1000 and 10000 m^{-1}). It can be noticed that the profiles from the two different modeling runs fit each other exactly, which constitutes a first validation of our model.

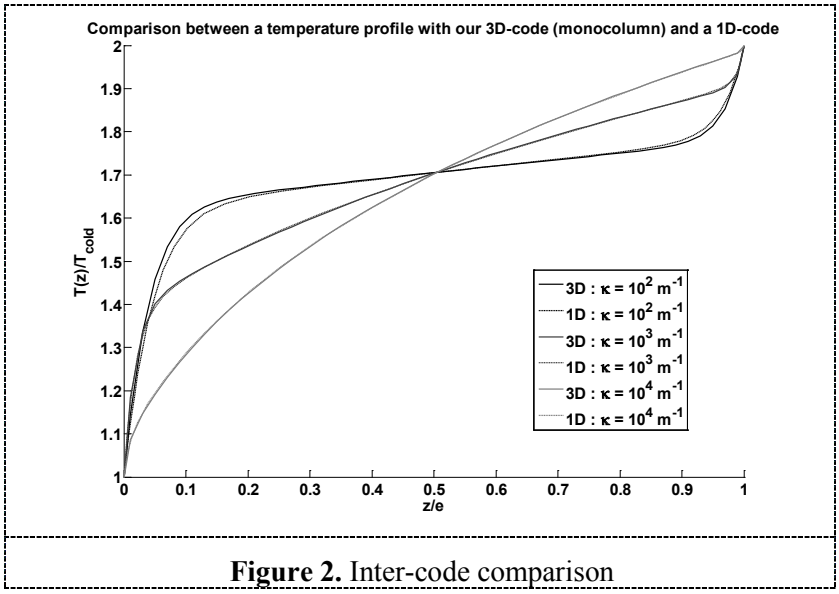

Figure 2. Inter-code comparison

We notice that the two profiles from the two different models are very close, which constitutes a first validation of our model. The low difference got for the low absorption coefficients is explained by the refined mesh near the walls taking into account in the 1D-model contrary to our model.

This study should be continued. The validations carried out during the progressive creation of the code (inter-codes or comparing with simplified versions for homogeneous media) have shown that this investigation is headed in the right direction. Future work involves validating the model with flash experiments on materials with different semi-transparency characteristics.

6. Conclusions

We have developed a calculation code in order to model the coupled conductive and radiative heat transfer within porous multiconstituent materials that are numerically represented by a numerical voxelized structure. This discretization corresponds to a very fine description of the morphology of the studied samples. The purpose of this work was to numerically simulate thermal experiments or the real behavior of the studied materials when subjected to any kind of thermal stress. The code was validated thanks to simplified conductive and radiative models solving the same problem in other ways. The next step will be to validate it by attempting to reproduce the real experimental behavior of materials of different characteristics.

References

[1] M. Niezgoda, D. Rochais, F. Enguehard, P. Echegut, B. Rousseau, Modeling of time-resolved coupled radiative and conductive heat transfer in multilayer semitransparent materials, *Appl. Phys. Lett.*, **99**, 224101 (2011).

[2] K. Boomsma, D. Poulikakos, On the effective thermal conductivity of a three dimensionally structured fluid saturated metal foams, *Int. J. Heat Mass Transfer*, **44** [4], 827–836 (2001).

[3] A. Bhattacharya, V.V. Calmidi, R.J. Mahajan, Thermophysical properties of high porosity metal foams, *Int. J. Heat Mass Transfer*, **45** [5], 1017–1031(2002).

[4] B.P. Singh, M. Kaviany, Modeling radiative heat transfer in packed beds, *Int. J. Heat Mass Transfer*, **35** [6], 1397–1405 (1992).

[5] J. Dombrovsky, H. Randrianalisoa, W. Lipinski, D. Baillis, Approximate analytical solution to normal emittance of semi-transparent layer of an absorbing, scattering, and refracting medium, *J. Quant. Spectrsc. Radiat. Transfer*, **112**, 1987–1994 (2011).

[6] S. André, A. Degiovanni, A new way of solving transient radiative–conductive heat transfer problems, *J. Heat Transfer*, **120**, 943–955 (1998).

[7] O. Hahn, F. Raether, M.C. Arduini-Schuster, J. Fricke, A. Degiovanni, Transient coupled conductive/radiative heat transfer in absorbing emitting and scattering media: application to laser-flash measurements on ceramic materials, *Int. J. Heat Mass Transfer*, **40** [3], 689–698 (1997).

[8] M. Lazard, S. André, D. Maillet, Diffusivity measurement of semi-transparent media: model of the coupled transient heat transfer and experiments on glass silica glass and zinc selenide, *Int. J. Heat Mass Transfer*, **47**, 477–487 (2004).

[9] R. Coquard, D. Rochais, D. Baillis, Experimental investigations of the coupled conductive and radiative heat transfer in metallic/ceramic foams, *Int. J. Heat Mass Transfer*, **52**, 4907–4918 (2009).

[10] A.M. Druma, M.K. Alam, C. Druma, Analysis of thermal conduction in carbon foams, *Int. J. Thermal Sci.*, **43** [7], 689–695 (2004).

[11] R. Coquard, M. Loretz, D. Baillis, Conductive heat transfer in metallic/ceramic open-cell foams, *Adv. Eng. Mater.*, **10** [4], (2008).

[12] R. Coquard, D. Baillis, Numerical investigation of conductive heat transfer in high-porosity foams, *Acta Mater.*, **57** [18], 5466–5479 (2009).

[13] M. Saadatfar, C.H. Arns, M.A. Knackstedt, T. Senden, Mechanical and transport properties of polymeric foams derived from 3D images, *Colloids Surf. A Physicochem. Eng. Aspects*, **263** [1–3], 284–289 (2004).

[14] M. Wang, N. Pan, Modeling and prediction of the effective thermal conductivity of random open-cell porous foams, *Int. J. Heat Mass Transfer*, **51** [5–6], 1325–1331 (2008).

[15] C.Y. Zhao, S.A. Tassou, T.J. Lu, Analytical considerations of thermal radiation in cellular metal foams with open cells, *Int. J. Heat Mass Transfer*, **51** [3–4], 929–940 (2008).

[16] J. Petrasch, P. Wyssb, A. Steinfeld, Tomography-based Monte Carlo determination of radiative properties of reticulate porous ceramics, *J. Quant. Spectrosc. Radiative Transfer*, **105** [2], 180–197 (2007).

[17] B. Zeghondy, E. Iacona, J. Taine, Determination of the anisotropic radiative properties of a porous material by radiative distribution function identification (RDFI), *Int. J. Heat Mass Transfer*, **49**, 2810–2819 (2006).

[18] M. Loretz, R. Coquard, D. Baillis, E. Maire, Metallic foams: radiative properties/comparison between different models, *J. Quant. Spectrosc. Radiative Transfer*, **109** [1], 16–27 (2008).

[19] B. Rousseau, D. De Sousa Meneses, P. Echegut, M. Di Michiel, J.-F. Thovert, Prediction of the thermal radiative properties of an x-ray m-tomographied porous silica glass, *Appl. Opt.*, **46** 4266–4276 (2007).

[20] R. Coquard, B. Rousseau, P. Echegut, D. Baillis, H. Gomart, E. Iacona, Investigations of the radiative properties of Al–NiP foams using tomographic images and stereoscopic micrographs, *Int. J. Heat Mass Transfer*, **55**, 1606–1619 (2012).

[21] A. Akolkar, J. Petrasch, Tomography based pore-level optimization of radiative transfer in porous media, *Int. J. Heat Mass Transfer*, **54** [23–24], 4775–4783 (2011).

[22] N. Vivet, S. Chupin, E. Estrade, T. Piquero, P.L Pommier, D. Rochais, E. Bruneton, 3D Microstructural characterization of a SOFC anode reconstructed by FIB tomography, *J. Power Sources*, **196** [18], 7541–7549 (2011).

[23] D. Rochais, G. Le Meur, G. Domingues, V. Basini, Microscopic thermal characterization of HTR particle layers, *Nuclear Engineering and Design* (2008).

[24] J.F. Brun, D. De Sousa Meneses, B. Rousseau, P. Echegut, Dispersion Relations and Phase Retrieval in Infrared Reflection Spectra Analysis, *Soc. Appl. Spect.*, **55** [6], 774–780 (2001).